Urban Radiowave Propagation: A 3-D Path-Integral Wave Analysis

Costas C. Constantinou, *Member, IEEE*, and Ling Chuen Ong

***Abstract*— A discussion concerning the need for three-dimensional (3-D) urban radiowave propagation models is presented and followed by a review of previously published work on this topic using the asymptotic path-integral technique. The limitations and advantages of this technique are explained and it is applied to study diffraction by a small number of canonical geometries. The validity of this technique is verified by comparison with controlled laboratory measurements taken at millimetric wave frequencies. Finally, its ability to classify field components according to their distribution in space is employed in order to analyze the observed field strength distributions in the model environments.**

***Index Terms*— Radio propagation.**

I. Introduction

A LARGE number of radiowave propagation models are two-dimensional (2-D) great circle path models [1], [2]. Such models mainly predict median field strength as a function of radial distance from the base station. Both empirical and deterministic propagation models specific to urban cellular mobile radio are undergoing an evolution from being 2-D [1]–[3] to simulating propagation in three dimensions [4]–[6].

The gradual decrease in cell dimensions geared toward accommodating higher mobile telephony user densities has lead to the proposal of employing microcells with base station antennas located well within the local environment [7]. The location of the base station antenna below the local building rooftops implies that the field strength dependence can no longer be adequately described in terms of a single radial distance variable since the streets have a fairly strong guiding effect. The models predominately used in microcellular propagation are based on ray-optical techniques [4]–[6]. These models tend not to be fully three-dimensional (3-D) as they either neglect propagation over rooftops [6] or additionally consider great circle path propagation over rooftops [4] but neglect off-great circle path propagation.

Microcellular mobile radio system designers will in future require accurate estimates of carrier to co-channel interference ratios in order to design interference-limited high-capacity mobile radio systems. The impact of prediction uncertainty in both the carrier and co-channel interferer field strength has been recently quantified by Koshi *et al*. [8]. It is known [9] that propagation modeling over short distances (and for antennas situated within the environmental clutter) needs to be 3-D. It is also frequently asserted [9] that propagation over relatively long distances typically occurs over rooftops, so it is predominantly 2-D great circle path energy transport. As the distances of the significant co-channel interferers in a microcellular scenario are likely to fall between the above two extreme cases, the need arises for fully 3-D propagation models that do not make *a priori* assumptions about significant energy transport paths.

In this paper, we present a full-wave analysis tool for studying 3-D diffraction problems in urban areas. The tool is not intended to be a fully fledged propagation prediction tool; instead, we use it in order to classify the relative magnitudes of fields that interact with various geometrical features of idealised 3-D objects. The work presented here represents an important first step in the systematic development of 3-D propagation models.

The paper is conceptually divided into three parts. Sections II and III summarize the asymptotic path integral technique and its applications and spell out its limitations and advantages. Sections IV, V, and VI present the theory and simulations, briefly describe the experiments, and discuss the results in detail. Finally, Section VII presents the conclusions drawn from this work.

II. Summary of the Asymptotic Path-Integral Technique and Its Previous Applications

The technique we choose to adopt to model 3-D radiowave propagation is the asymptotic path-integral technique [10], which is known to be equivalent to the scalar Fresnel–Kirchhoff diffraction theory [11]. Details of the asymptotic path-integral formalism are given in Eliades [10] and Ong and Constantinou [12] and will not be repeated here for the sake of brevity. The computational aspects of the use of the asymptotic path-integral technique are dealt with in a separate paper [13].

We summarize here some important results and conclusions originally presented at the fifth IEEE International Symposium on Personal, Indoor, and Mobile Radio Communications by the authors [14] in order to demonstrate the large discrepancies that can arise in modeling 3-D diffracting obstacles by equivalent lower dimensional structures such as knife edges. The conclusions, which were verified through controlled scaled-frequency measurements [14] were as follows.

1) Modeling infinite-width cascaded plateaux by infinite-width knife edges yields an accurate result for the

Manuscript received October 29, 1996; revised June 30, 1997. This work was supported by EPSRC under Grant GR/H39543. L. C. Ong was supported by an IEE Postgraduate Scholarship.

The authors are with the School of Electronic and Electrical Engineering, The University of Birmingham, Edgbaston, Birmingham B15 2TT U.K.

Publisher Item Identifier S 0018-926X(98)01489-6.

attenuation function provided each knife edge is of the same height and is placed at the center of each plateau.

2) Modeling finite-width cascaded plateaux by finite-width knife edges can give rise to significant errors in the calculation of the attenuation function, provided the field strength that diffracts over the top of each obstacle is within two orders of magnitude of the field strength that diffracts around its sides. The equivalent knife-edge modeling errors were found to be as high as 20 dB in the cases examined.
3) In environments where the transmitter–receiver separations are typically small or at least comparable to obstacle widths, propagation models need to be 3-D in order to produce reliable predictions.

As a consequence, it can be seen that the cascaded knife-edge diffraction models of the macrocellular urban environment [2], [15] must be used with care as any approximately radial road gaps in the skyline close to the great circle path are likely to be ignored in the modeling process and lead to significant prediction errors. The modeling errors are likely to be even more severe in the microcellular scenario, but this remains to be proven.

III. Limitations and Advantages of the Asymptotic Path-Integral Technique

The asymptotic path-integral technique used in this work possesses a number of limitations and advantages that should be borne in mind when examining the results we discuss in this paper. Therefore, a short outline of these is presented here.

The path-integral technique was originally developed by Feynman [16] as an alternative interpretation of nonrelativistic quantum mechanics, but has since found widespread applications in many other areas of physics [17], including electromagnetics [18], [19]. However, its domain of validity is restricted by the paraxial approximation [20], and in taking into account the polarization dependence of reflection coefficients as well as real material boundaries heuristic extensions need to be made to its formulation [10], [21].

The asymptotic version of the technique [10], [21] is known to suffer from the same formal inconsistencies and limitations as Fresnel–Kirchhoff diffraction theory [22], but its predictions were found to produce very good agreement in comparison to detailed laboratory measurements at microwave frequencies [21]. Finally, the asymptotic path-integral technique has only been applied to piecewise planar 3-D obstacle diffraction and the aperture field integrations the technique requires need to be performed along planes which are coincident with the faces of the objects. This final requirement renders the method very difficult to automate.

The advantages of the asymptotic path-integral technique are also considerable. The ability to count both ray-optical paths as well as apertures provides a more natural framework (albeit not unique to this technique) in which to describe quantitatively field interactions with individual segments of the object surfaces and energy transfer over individual aperture segments, examples of which will be presented below. The ability to readily describe energy propagation over individual spatial domains renders this method an excellent research tool which can, in principle, be used to determine the validity of 2-D [2] or limited 3-D [4], [6] propagation models.

IV. Simulations

The attenuation function for generic multiple piecewise-planar 3-D obstacles described by $(N+1)$ segments along the direction of propagation (here chosen to be the x axis) can be written as [21]

$$\begin{aligned} &A(N+1;0) \\ &= \left[\frac{jk}{2\pi}\right]^N \frac{(x_{N+1}-x_0)}{\prod_{n=0}^{N}(x_{n+1}-x_n)} e^{jk\frac{(y_{N+1}-y_0)^2+(z_{N+1}-z_0)^2}{2(x_{N+1}-x_0)}} \\ &\quad \times \sum_{m_N=0}^{1} \cdots \sum_{m_0=0}^{1} \rho^{\Sigma_{n=0}^{N} m_n} \sum_{m'_{N-1}=0}^{1} \cdots \sum_{m'_1=0}^{1} \rho'^{\Sigma_{n=1}^{N-1} m'_n} \\ &\quad \times \int_{S_N} dy_N\, dz_N \cdots \int_{S_1} dy_1\, dz_1 \\ &\quad \times e^{-jk\sum_{n=0}^{N}\frac{[(y_{n+1}+M_n y_n)^2-4m_n f_n]+[(z_{n+1}+M'_n z_n)^2-4m'_n g_n]}{2(x_{n+1}-x_n)}} \end{aligned} \tag{1}$$

where the surface of integration S_n is carried out over the area not blocked by the presence of the obstacles. In the above equation, w_n is the y coordinate of a possible vertical discontinuity in the nth aperture plane of the piecewise-planar profile, v_n is similarly the horizontal discontinuity, and

$$\begin{aligned} &M_n = 2m_n - 1; \quad M'_n = 2m'_n - 1; \quad m'_0 = m'_N = 0 \\ &f_n = w_{n+1}y_n + w_n y_{n+1} - w_n w_{n+1} \\ &g_n = v_{n+1}z_n + v_n z_{n+1} - v_n v_{n+1}. \end{aligned} \tag{2}$$

The reflection coefficient at the vertical faces (depends on chosen polarization) is denoted by ρ' while the corresponding reflection coefficient for horizontal faces is denoted by ρ. The separable nature of the integrals in (1) implies that provided the limits of integration are chosen appropriately, the integrations over the sets of variables y_n and z_n can be evaluated separately, each as a single one-dimensional integral described in detail by Ong [21].

Selecting each integral in the multiple summation above corresponds to selecting the field component interacting with the appropriate combination of boundaries, as becomes evident by the ρ and ρ' factors multiplying the above integral (see for example [12]). On the other hand, segmenting the apertures $\{S_i\}$ into smaller apertures yields field components that propagate in specific spatial regions (e.g., over the top of obstacles or around the sides).

Four distinct 3-D scattering geometries have been simulated with a fixed transmitter and a mobile receiver. The geometries and receiver trajectory are shown in Figs. 1 and 2. The field components are defined such that the "top" field component is the one propagating in the infinitely wide apertures above the obstacle heights, while the "side" field component is the one propagating in the infinitely high apertures above the

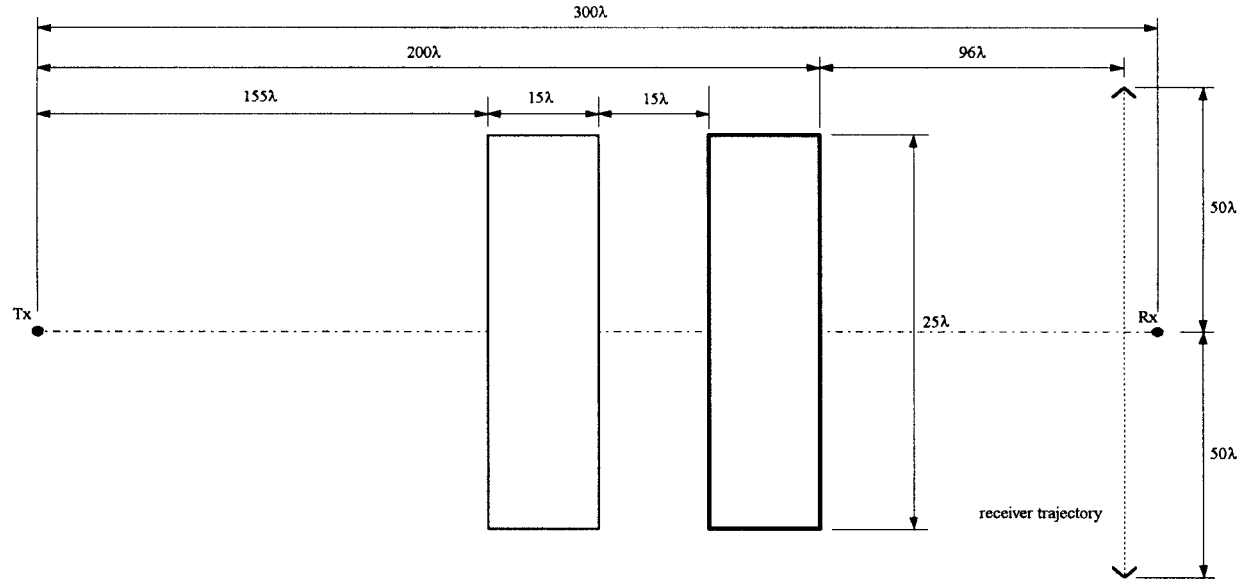

Fig. 1. Path geometry for the nonline-of-sight model (boldface lines indicate single obstacle scenario).

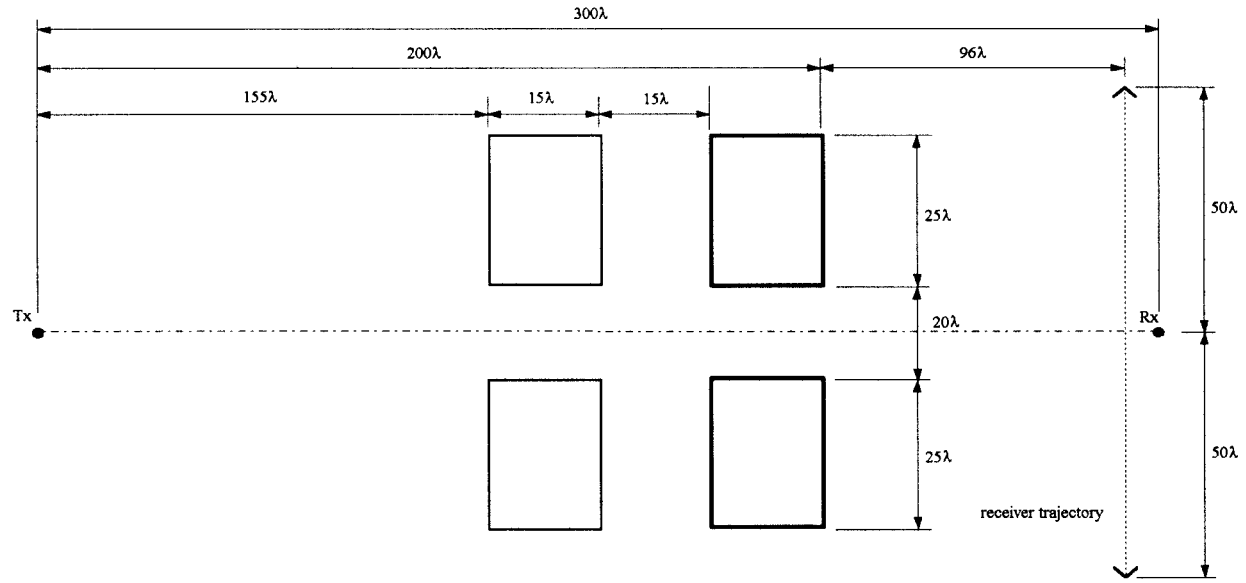

Fig. 2. Path geometry for the line-of-sight model (boldface lines indicate scenario with single row of obstacles).

ground and to the left or right of each finite-width obstacle. The quadrant-shaped aperture which exits to the side and above the obstacles is common to both definitions and is *not* counted twice when the total field is computed. It is precisely this component that is ignored in some limited 3-D diffraction models [4] and can potentially give rise to errors. The further classification in terms of interactions is such that direct (denoted by "d" in subsequent figures) refers to the field component that is independent of ρ and ρ', while interacting or reflected (denoted by "r" in subsequent figures) refers to the field component that depends on ρ and/or ρ'.

Thus, a caption term in Figs. 3–6 such as s1(d, r, d) is a shorthand notation for the field component corresponding energy transport on side 1 of the obstacle (the left-hand side) where there is direct transport of energy between the transmitter and the first aperture, reflected energy off a (side) boundary between the two apertures and direct transport of energy between the second aperture and the receiver.

V. Experiments

The experiments are carried out at millimetric frequencies in the laboratory using idealized obstacles. The obstacles and ground plane are constructed from aluminum sheets and the propagation range is surrounded with microwave absorbing material (Eccosorb VHP 8-NRL) to suppress unwanted energy scattering from the outside environment. A 30-GHz continuous wave signal is transmitted through a +18.2 dBi A-band horn antenna. The receiving antenna is an open-ended single-mode rectangular waveguide having a boreside gain of +8.2 dBi. The measurement accuracy is ±1 dB throughout, and both the

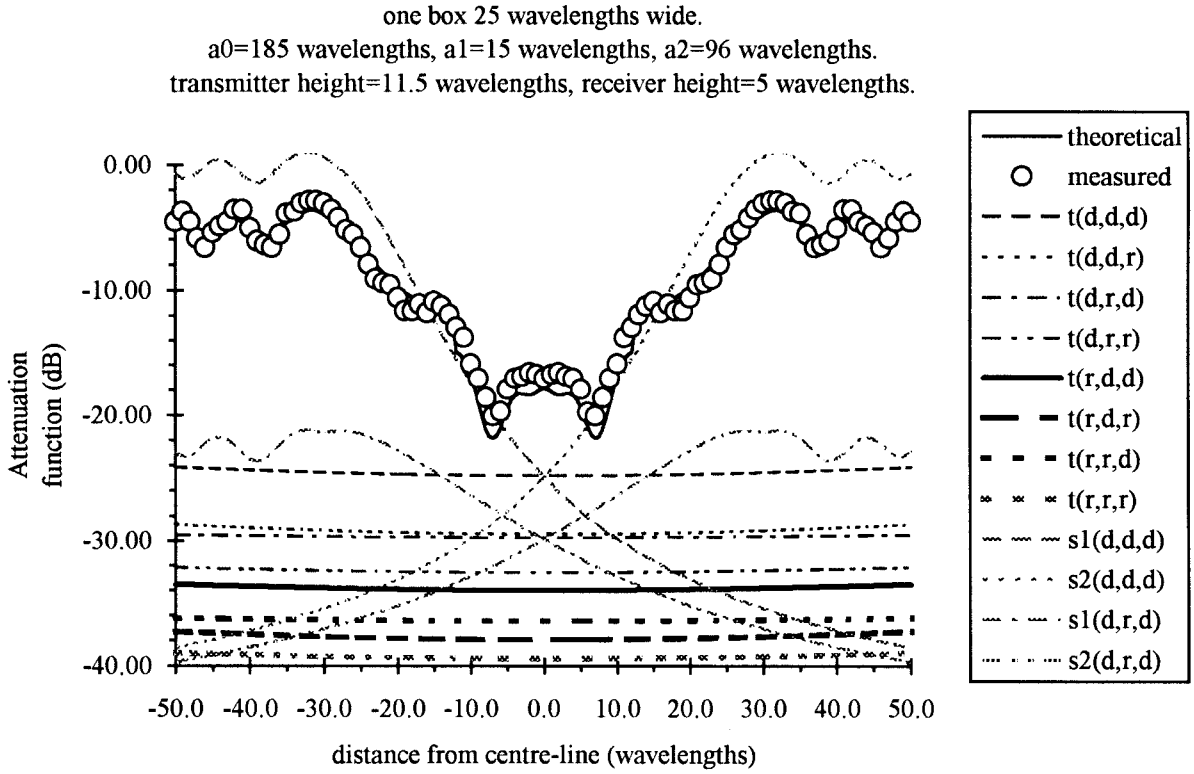

Fig. 3. Attenuation function for one box of 25 λ width for transmitter height of 11.5 λ with the receiver moving in the transverse direction (nonline-of-sight), (t: top; s1: left side; s2: right side; d: direct, r: reflected fields).

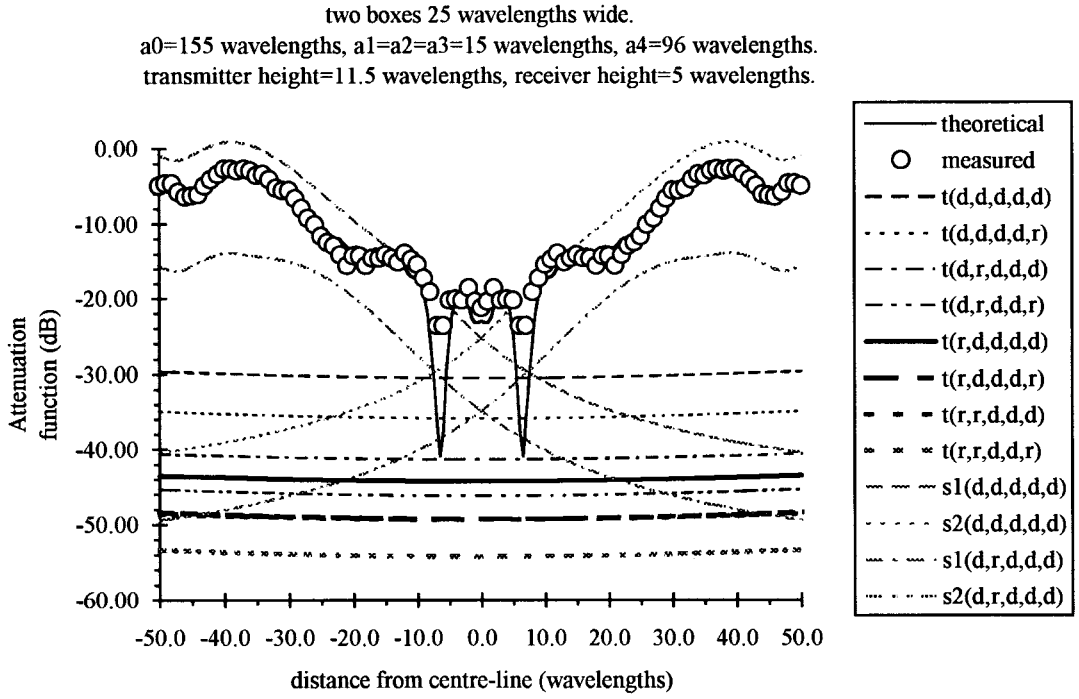

Fig. 4. Attenuation function for two boxes of 25 λ width for transmitter height of 11.5 λ with the receiver moving in the transverse direction (nonline-of-sight), (t: top; s1: left side; s2: right side; d: direct, r: reflected fields).

measurements and simulations are normalized with respect to free-space field strength.

Vertical polarization is adopted in the experiments for which $\rho = 1$ and $\rho' = -1$. The height of the transmitter is kept constant at 11.5 λ throughout. Since the height of all the obstacles used is 20 λ, the experimental setup corresponds to the microcellular environment in which the transmitters are located below the rooftop level of the surrounding buildings.

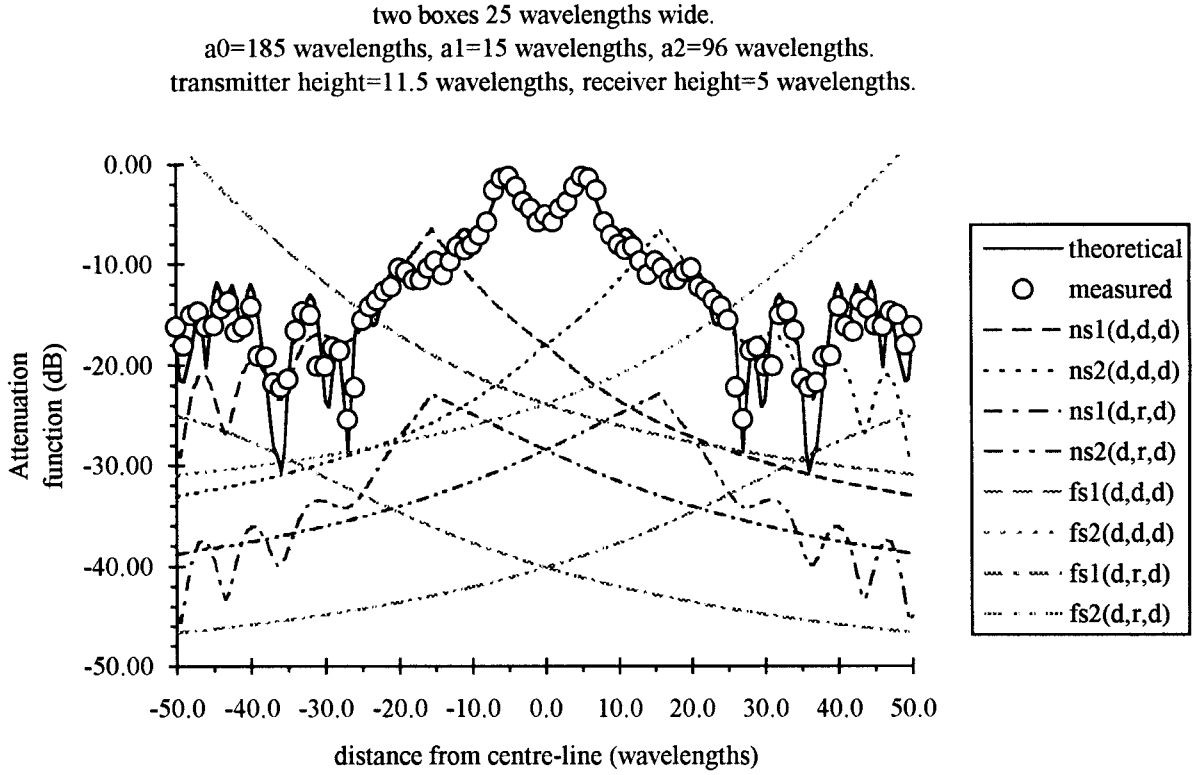

Fig. 5. Attenuation function for two boxes of 25 λ width for transmitter height of 11.5 λ with the receiver moving in the transverse direction (line-of-sight) (ns1: near/inner side of left box; fs1: far/outer side of left box; ns2: near/inner side of right box; fs2: far/outer side of right box; d: direct, r: reflected fields).

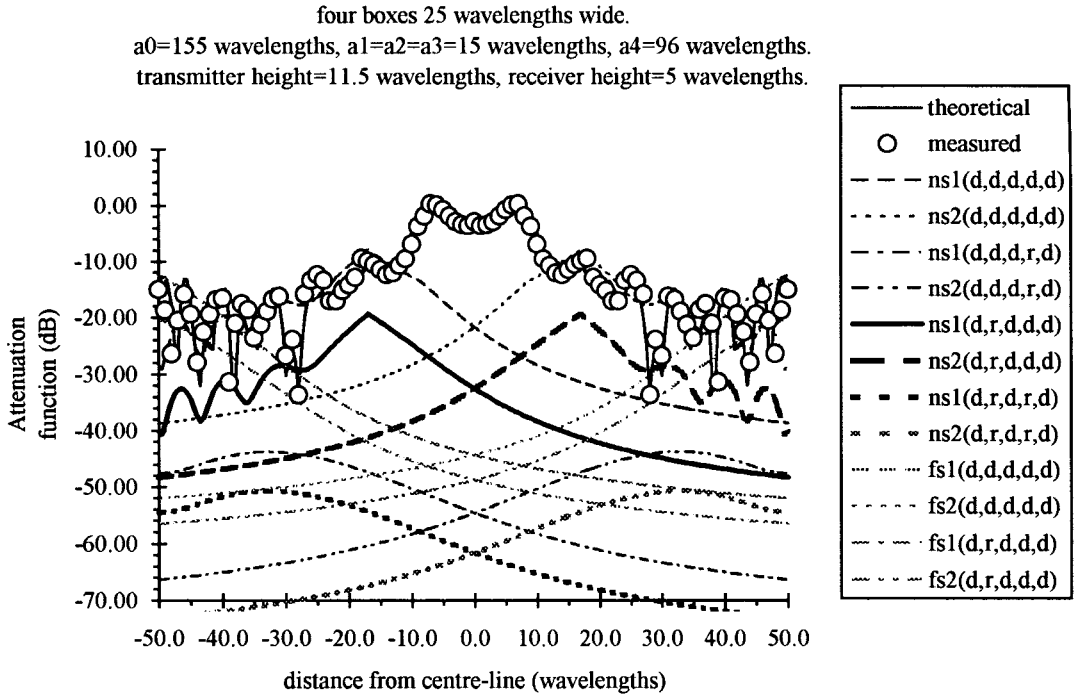

Fig. 6. Attenuation function for four boxes of 25 λ width for transmitter height of 11.5 λ with the receiver moving in the transverse direction (line-of-sight) (ns1: near/inner side of left box; fs1: far/outer side of left box; ns2: near/inner side of right box; fs2: far/outer side of right box; d: direct, r: reflected fields).

The receiver height is 5 λ above the ground plane and its trajectory is shown in Figs. 1 and 2; it extends from -50 λ to 50 λ along the perpendicular to the line of symmetry, located at a distance of 296 λ from the transmitter.

VI. Discussion of Results

The transverse movement of the receiver both in the line-of-sight and nonline-of-sight scenarios depicted in Figs. 1 and 2 will be examined in this section. The

geometric arrangement details were described in the last section.

The attenuation function normalized with respect to free-space for a box of 25 λ width and 15 λ length positioned symmetrically about the central propagation path is shown in Fig. 3. In this arrangement, the leading face of this box-shaped obstacle is 185 λ from the transmitter. The agreement between theory and measurement is excellent (rms error of 1 dB). The field strengths relative to the free-space field strength are also plotted in the figure for the main top path components. This class of path components must be included in the calculations of the attenuation functions for the plateau models as in certain locations (e.g., shadow region) they are well within a few decibels of the side-diffracted signals. The side path components propagating directly across and reflected off the sides are also plotted in the graphs. The total attenuation function is characterized by small ripples in the shadow region due to interference between the various field components and the side-diffracted field components possess the familiar Fresnel function form as the receiver moves into the lit region. In the latter location, the contributions arise principally from the side-diffracted path components from the plateau edges nearer to the receiver. At receiver positions of ± 20 λ for the 25-λ-wide plateau, the vertical side faces of the boxes are in the first Fresnel zone. At these receiver positions, the path components arising from the vertical face of the plateau furthest from the receiver can be ignored as these are many orders of magnitude weaker (by at least 25 dB) than the components diffracting from the nearer plateau face.

In similar simulations for a knife edge (not presented here for brevity) there exists only one dominant side-field component in the lit regions (there is no interacting side component). The top ground-reflected field components are found to be significantly weaker than the equivalent top interacting field components in the case of the plateau. This results explain the inconsistencies in modeling plateaux by knife edges reported in [14].

The single plateau problem is now extended to that of two rows of 20-λ-high plateaux by adding a second identical plateau between the first one and the transmitter. The distance from the transmitter to its nearest plateau illuminated face is now 155 λ. The top path components that interact with the top of the second plateau and those that are ground-reflected between the plateaux are not shown in Fig. 4, as their field strengths are significantly lower than those of the main top path components. Likewise, the side path components that interact with the side of the second plateau and those that are cross diffracted between the plateaux are also neglected for the same reason. Once again, the contributions are primarily due to the side-diffracted path components arising from the plateau face nearest to the receiver as it moves into the lit region. The disagreement between predictions and measurements in the region of deep nulls results in relatively high-error statistics (rms error of 3 dB). This is due to the fact that we have neglected the weak components described above in our simulations. Otherwise, the agreement is very good elsewhere.

The line-of-sight scenario depicted in Fig. 2 is examined next. This layout is a simplified representation of a street intersection. The attenuation function for two 25-λ-wide and 15-λ-long plateaux positioned symmetrically on either side of the central propagation path is shown in Fig. 5. The dominant field components in the lit region are the direct and ground-reflected ones. As the receiver moves out of the shadow region and into the lit region, the contributions arise mainly from the interference of all the side-diffracted path components.

The agreement between theory and measurement is good. The receiver is still in the shadow region up to receiver positions at ± 51.8 λ for the 25-λ-wide plateau arrangement. In this region, the depths of the ripples are small and the predictions agree well with the measurements (rms error of 2.5 dB).

The single row of plateaux is now extended to two rows. The transmitter is now 155 λ away from its nearest plateau. The cross-diffracted components between rows of plateaux were neglected because of their significantly weaker field strengths (by at least 30 dB compared to all other components). The attenuation function for the two rows of 25-λ-wide plateaux is plotted in Fig. 6. The total field strength in the shadow regions is observed to be much higher than that for the single row of plateaux arrangements. The receiver now has to travel a longer distance before it enters into the lit regions. For distances between ± 66.8 λ for the 25-λ plateau arrangement, the receiver can be seen to still be in the shadow regions. The agreement between the predictions and measurements remains good (rms error of 3.3 dB).

VII. Summary and Conclusions

The asymptotic path-integral technique has been applied successfully to the study of diffraction from 3-D idealized obstacles and its prediction accuracy has been verified experimentally.

A brief review of diffraction by cascaded 3-D obstacles and their representation in terms of equivalent knife edges (of both infinite and finite width) has lead to the conclusion that in accurately modeling radiowave propagation in the urban environment, 3-D diffraction processes need to be considered explicitly.

The ability of the asymptotic path-integral technique to simultaneously distinguish between field-component spatial distributions as well as interactions has also been demonstrated. Therefore, the potential value of this technique as a research tool to be used in identifying dominant propagation paths in the urban environment and thus enhancing our understanding of propagation mechanisms now becomes evident. Such insights into propagation mechanisms can potentially lead to the development of efficient and accurate 3-D urban radiowave propagation models, which will be essential for the planning of high-density mobile telephony services. Research in this area is ongoing at Birmingham University, U.K.

Acknowledgment

The authors would like to thank the Radiocommunications Agency and Defense Research Agency for the long-term loan of equipment.

REFERENCES

[1] M. Hata, "Empirical formula for propagation loss in land mobile radio service," *IEEE Trans. Veh. Technol.*, vol. VT-29, pp. 317–325, Aug. 1980.

[2] J. Walfisch and H. L. Bertoni, "A theoretical model of UHF propagation in urban environments," *IEEE Trans. Antennas Propagat.*, vol. 36, pp. 1788–1796, Dec. 1988.

[3] COST 207, "Digital land mobile radio communications, final report of the COST 207 management committee," presented at Directorate-Gen. Telecommun., Inform. Indust. Innovation, Commission Eur. Communities, Luxembourg, 1989.

[4] T. Kurner, D. J. Cichon, and W. Wiesbeck, "Concepts and results for 3-D digital terrain-based wave propagation models; An overview," *IEEE J. Select. Areas Commun.*, vol. 11, pp. 1002–1012, Sept. 1993.

[5] T. S. Rappaport and S. Sandhu, "Radio-wave propagation for emerging wireless personal-communication systems," *IEEE Antennas Propagat. Mag.*, vol. 36, pp. 14–23, Oct. 1994.

[6] G. E. Athanasiadou, A. R. Nix, and J. P. McGeehan, "A ray tracing algorithm for microcellular and indoor propagation," in *9th Inst. Elect. Eng. Int. Conf. Antennas Propagat.*, Chicago, IL, July 1995, vol. 2, pp. 231–235.

[7] M. J. Mehler, "The microcell propagation challenge," *Inst. Elect. Eng. Colloq. Microcellular Propagat. Modeling*, London, U.K., 1992, vol. 1992/234, pp. 1/1–1/4.

[8] V. Koshi, D. J. Edwards, A. M. Street, and M. J. Mehler, "Impact of planning uncertainties in designing a cellular mobile communication network," in *Proc. IEEE Veh. Technol. Conf.*, Phoenix, AZ, May 1997, pp. 775–779.

[9] H. L. Bertoni, W. Honcharenko, L. R. Maciel, and H. H. Xia, "UHF propagation prediction for wireless personal communications," in *Proc. IEEE*, Sept. 1994, vol. 82, pp. 1333–1359.

[10] D. E. Eliades, "Path integral analysis of paraxial radiowaves propagation over a nonlevel plateau," *Proc. Inst. Elect. Eng.*, vol. 138, pt. H, pp. 521–526, Dec. 1991.

[11] J. H. Whitteker, "A series solution for diffraction over terrain modeled as multiple bridged knife-edges," *Radio Sci.*, vol. 28, pp. 487–500, 1993.

[12] L. C. Ong and C. C. Constantinou, "Diffraction over an infinitely wide plateau," *Proc. Inst. Elect. Eng. Microwaves Antennas Propagat.*, vol. 143, pp. 94–96, Feb. 1996.

[13] ———, "Evaluation of multiple diffraction integrals: Computational speed and accuracy considerations," *Proc. Inst. Elect. Eng. Microwaves Antennas Propagat.*, vol. 144, pp. 35–41, Feb. 1997.

[14] C. C. Constantinou and L. C. Ong, "Use of zero vs. nonzero thickness diffracting obstacles in radio channel modeling," in *5th IEEE Int. Symp. PIMRC*, The Hague, Sept. 1994, pp. 280–286.

[15] M. J. Neve and G. B. Rowe, "Mobile radio propagation prediction in irregular cellular topographies using ray methods," *Proc. Inst. Elect. Eng. Microwaves Antennas Propagation*, vol. 142, pp. 447–451, Dec. 1995.

[16] R. P. Feynman and A. R. Hibbs, *Quantum Mechanics and Path Integrals*. New York: McGraw-Hill, 1965.

[17] L. S. Schulman, *Techniques and Applications of Path Integration*. New York: Wiley, 1981.

[18] S. W. Lee, "Path integrals for solving some electromagnetics edge diffraction problems," *J. Math. Phys.*, vol. 19, pp. 1414–1422, 1978.

[19] C. Huang, "Path integral method in classical electromagnetics," Ph.D. dissertation, Texas A&M University, College Station, TX, 1992.

[20] C. C. Constantinou, "Path-integral analysis of passive, graded-index waveguides applicable to integrated optics," Ph.D. dissertation, Univ. Birmingham, 1991.

[21] L. C. Ong, "Radiowave propagation in urban environments," Ph.D. dissertation, Univ. Birmingham, 1995.

[22] G. Barton, *Elements of Green's Functions and Propagation*. Oxford, U.K.: Oxford Univ., 1989.

Costas C. Constantinou (M'91) received the B.Eng. (honors) degree in electronic and communication engineering and the Ph.D. degree in electronic and electrical engineering from the University of Birmingham, U.K., in 1987 and 1991, respectively.

From 1989 to the present, he has been a Lecturer in Communications in the School of Electronic and Electrical Engineering at the University of Birmingham, U.K. and since 1991 he has headed the radiowave propagation research program in the Communications Engineering Research Group at the same university. His research interests include optical communications, electromagnetic theory, deterministic radiowave propagation modeling, and mobile radio.

Dr. Constantinou is a member of the British Telecom Virtual University Research Initiative on Mobility.

Ling Chuen Ong received the B.Eng. (honors) degree in electronic and communication engineering and the Ph.D. degree in electronic and electrical engineering from the University of Birmingham, U.K., in 1992 and 1996, respectively.

From 1992 to 1995, he worked as a Research Associate at the University of Birmingham on a Science and Engineering Research Council (now EPSRC) grant. Currently he is a Planning Manager with Singapore Telecom Pte. Ltd.